ACS central science

Research Article

Cite This: ACS Cent. Sci. 2019, 5, 486−493

http://pubs.acs.org/journal/acscii

Using Microfluidics and Imaging SAMDI-MS To Characterize Reaction Kinetics

Jennifer Grant,[†,∥] Patrick T. O'Kane,[†,∥] Blaise R. Kimmel,[‡] and Milan Mrksich*[,†,§]

[†]Department of Chemistry, [‡]Department of Chemical & Biological Engineering, and [§]Department of Biomedical Engineering, Northwestern University, Evanston, Illinois 60208, United States

Supporting Information

ABSTRACT: Microfluidic platforms have enabled the simplification of biochemical assays with a significant reduction in the use of reagents, yet the current methods available for analyzing reaction products can limit applications of these approaches. This paper demonstrates a simple microfluidic device that incorporates a functionalized self-assembled monolayer to measure the rate constant for a chemical reaction. The device mixes the reactants and allows them to selectively immobilize to the monolayer at the base of a microfluidic channel in a time-dependent manner as they flow down the channel. Imaging self-assembled monolayers for matrix-assisted laser desorption/ionization mass spectrometry (iSAMDI-MS) is used to acquire a quantitative image representing the time-resolved progress of the reaction as it flowed through the channel. Knowledge of the surface immobilization chemistry and the fluid front characteristics allows for the determination of the chemical reaction rate constant. This approach widens the applicability of microfluidics for chemical reaction monitoring and establishes a label-free method for studying processes that occur within a dispersive regime.

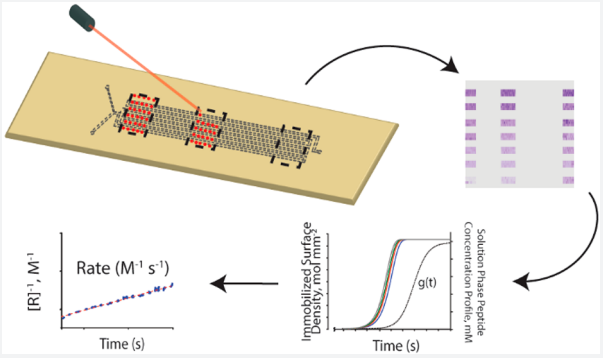

INTRODUCTION

Microfluidic systems have shown unprecedented levels of precision, miniaturization, and operational control over traditional benchtop and batch-based reactions. For example, Hollfelder and co-workers used electrocoalescence to fuse two droplets containing the reactant and recorded the reaction progress with a camera operating at 2 kHz to analyze a chemical reaction with a rate constant ∼3 × 10^4 M^{-3} s^{-1}.[1] Microfluidic devices have also been designed to screen reaction conditions. Cremer and co-workers developed a device that can generate a linear temperature gradient across many parallel microfluidic channels and showed that it can screen 36 temperatures for the synthesis of CdSe nanocrystals, as well as other applications.[2] However, analysis of reaction progress in microfluidic devices has been mainly limited to optical methods, which require the use of fluorescent or UV-absorbing products that limit applicability toward a small subset of chemical reactions.

Mass spectrometry is a powerful analytical technique that, when properly integrated with fluidics, can address these limitations by analyzing mixtures of compounds without the need for labels in a straightforward way. Recently described approaches have coupled microfluidic outlet streams directly to ESI-MS[3−5] or combined matrix with outlet droplets for subsequent analysis by MALDI-MS.[6−8] These methods highlight the benefits of integrating unbiased detection strategies with microfluidics to provide high-throughput experimental data. However, ESI-MS and MALDI-MS require sampling an appreciable volume from the reactor outlet, and salts (as well as some solvents) adversely affect instrument performance, thus sacrificing sensitivity and temporal resolution on product conversion. Mass spectrometric approaches that are sensitive, are high-throughput, and do not require product workup will present new opportunities for on-chip chemical reaction monitoring.

In this paper, we use imaging self-assembled monolayers for matrix-assisted laser/desorption ionization mass spectrometry (iSAMDI-MS) to describe the kinetic profile of a chemical reaction. In contrast to typical applications of fluidic approaches that sample product from the outlet stream or use optical tools for measuring reaction progress, we designed a device that incorporates a chemically defined self-assembled monolayer on the floor of the channel that can be directly analyzed with a MALDI-TOF mass spectrometer. This monolayer is functionalized to covalently bind the reactant and product from the flow above; therefore, it samples the reaction mixture as it flows through the microfluidic channel. The monolayer therefore collects a spatiotemporal record of the reaction, which can later be read and quantified using iSAMDI-MS. We also show how models of the dispersion front of the flow were necessary to analyze the images and extract the second-order rate constants for the reaction. In the example we present here, we quantified 15 720 data points

Received: November 26, 2018
Published: February 12, 2019

DOI: 10.1021/acscentsci.8b00867
ACS Cent. Sci. 2019, 5, 486−493

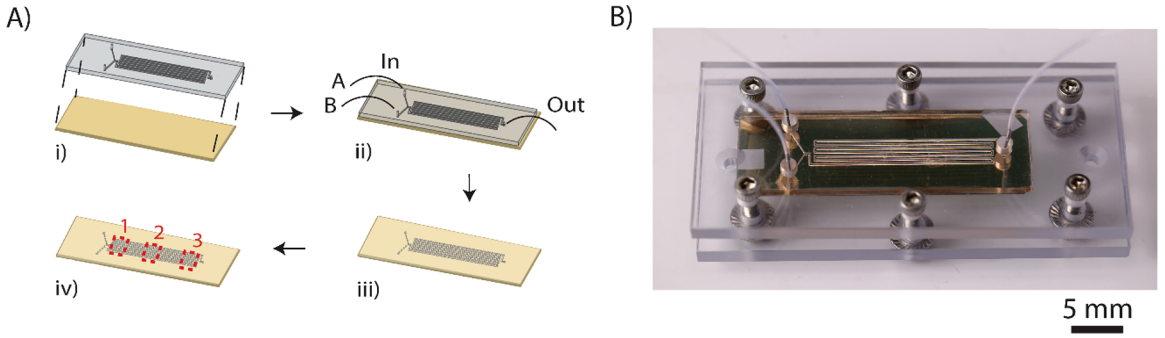

Figure 1. (A) Design and operation of the microfluidic device. (i) A poly(dimethylsiloxane) (PDMS) structure having channels in relief is joined to a gold-coated slide functionalized with self-assembled monolayer. (ii) Reactants A and B are simultaneously injected into the respective inlets and allowed to flow through the serpentine channel, during which reactant and product undergo immobilization to the monolayer. (iii) The PDMS chip is removed, and matrix is applied to the slide. (iv) iSAMDI-MS is used to quantitate immobilized reactant and product in three regions on the slide. (B) A photograph of the microfluidic chip and clamp assembly.

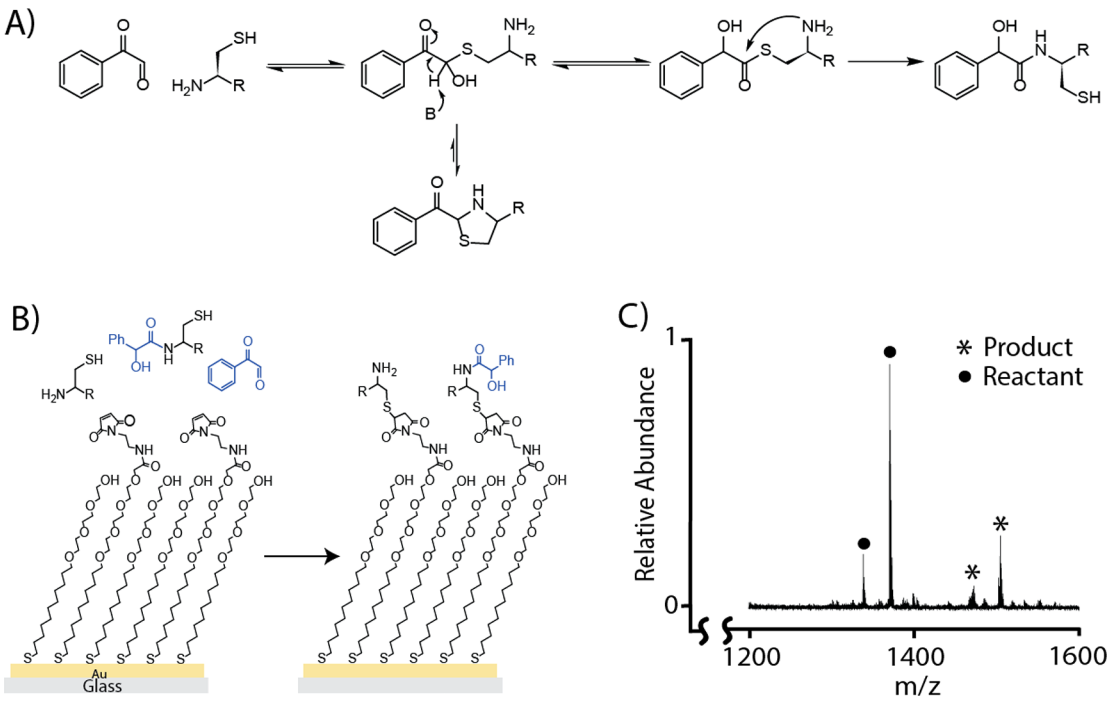

Figure 2. (A) Mechanism for the ligation reaction studied in this work. (B) Self-assembled monolayer presenting maleimide groups reacts with the cysteine-terminated peptide and its adduct. (C) SAMDI-MS spectrum of the monolayer after immobilization shows peaks corresponding to the reactant and product.

using only 160 μL of reagent, and we determine the pH-dependent rate constants for a chemical reaction.

DESIGN RATIONALE

We designed a microfluidic device for monitoring the progress of a chemical reaction, as described in Figure 1. The device has two inputs—one for each reactant—that diffusively mix at the base of a Y-junction and travel along the length of a single, unidirectional channel. The floor of the microfluidic device is functionalized with a self-assembled monolayer that covalently immobilizes the thiol-containing reactant and product by reaction with a maleimide group on the monolayer.[9] In this way, the monolayer records the reaction progress, and the distance from the Y-junction corresponds to the reaction time. Removal of the microfluidic cassette from the bottom substrate reveals the monolayer that contains a spatiotemporal record of reaction progress, which can be analyzed by iSAMDI-MS.

RESULTS

Peptide Ligation Reaction. We recently identified a novel chemical ligation reaction in which an α-keto aldehyde reacts with a peptide containing an N-terminal cysteine residue to join the two molecules by way of an α-hydroxy-amide bond (Figure 2A). This reaction can be understood from previous work that showed methylglyoxal reacts with free thiols in aqueous solution to generate a lactyl thioester.[10,11] We observed that the corresponding reaction with a peptide having an N-terminal cysteine underwent subsequent intramolecular acyl transfer to generate the amide product, in analogy to native ligation reactions.[12]

In the work described below, we use phenylglyoxal because it lacks enolizable protons that could lead to side products (Figure 2A). Also important in our work, both the reactant peptide and ligation product contain a free thiol that enables them to be covalently captured onto the maleimide-function-

DOI: 10.1021/acscentsci.8b00867
ACS Cent. Sci. 2019, 5, 486−493

alized self-assembled monolayer for detection (Figure 2B). We note that these species may also reversibly form a thiazolidine ring, which is observable by MALDI-TOF mass spectrometry of the reaction mixture but is not observed by SAMDI-MS because it does not contain a free thiol for immobilization (Figure S1). The SAMDI-MS spectra of the ligation reaction show peaks corresponding to immobilization of the unreacted peptide and the ligation product (Figure 2C).

Microfluidic Device Design and Operation. We performed the peptide ligation reaction in a poly(dimethylsiloxane) (PDMS) microfluidic device containing a Y-shaped microfluidic channel with two inlets and one outlet. We cast the PDMS block from 3D printed masters to avoid the use of a cleanroom and to enable rapid design prototyping (Figure S2).[13] Separate solutions of phenylglyoxal and the peptide, each at a concentration of 2 mM, were simultaneously injected into separate inlets and allowed to diffusively mix at the base of a Y-junction, where they continued to react as the solution flowed along a single channel that was 340 mm long, 550 μm wide, and 250 μm tall. In the flow, we included a peptide (0.25 mM) lacking an N-terminal cysteine that is unable to undergo internal rearrangement to form the permanent hydroxy-amide bond. This served as an internal standard for monitoring imaging performance and consistency. The thiol-containing peptide reactant, hydroxy-amide ligated product, and calibrant underwent immobilization to the monolayer as the fluid front flowed down the channel. The monolayer presents maleimide at a density of 20% relative to a tri(ethylene glycol) background, and once saturated, it serves as a record of the reaction profile from the channel. After flowing the reactants through the device, we removed the PDMS block from the chip and applied matrix to the chip as previously described.[14]

We used imaging mass spectrometry (iSAMDI-MS) to generate mass intensity maps of the molecules immobilized to the monolayer, as described by us recently.[14] iSAMDI-MS acquires individual SAMDI-MS spectra corresponding to each pixel, where each pixel (i.e., spectrum) reports the chemical composition of the fluid above the self-assembled monolayer. The resulting data set therefore serves as a spatial map of mass spectra containing maleimide-terminated alkanedisulfides functionalized with the reactant and product, and which represent the extent of reaction at each position in the channel. These pixels correspond to a distinct reaction time (depending on the position down the channel and the flow rate in the channel) and therefore provide a kinetic profile for the reaction (Figure 3A). Here, we used iSAMDI-MS to image three regions by acquiring spectra in reflector positive mode with a 200 μm lateral resolution. We performed experiments where the pH of the buffer was either 6.8, 7.2, 7.6, or 8.0; the spatial maps of product conversion at each pH are plotted in Figure 3B. The fractional yield of product was calculated using eq 1:

$$\text{fractional yield} = \frac{I_P}{I_P + I_S} \quad (1)$$

where I_P is the monoisotopic peak intensity of the product−maleimide alkanedisulfide conjugate, and I_S is the monoisotopic peak intensity of the reactant−maleimide alkanedisulfide conjugate. Each iSAMDI-MS data set includes approximately 1200 individually addressable reactions that occurred in the microfluidic device.

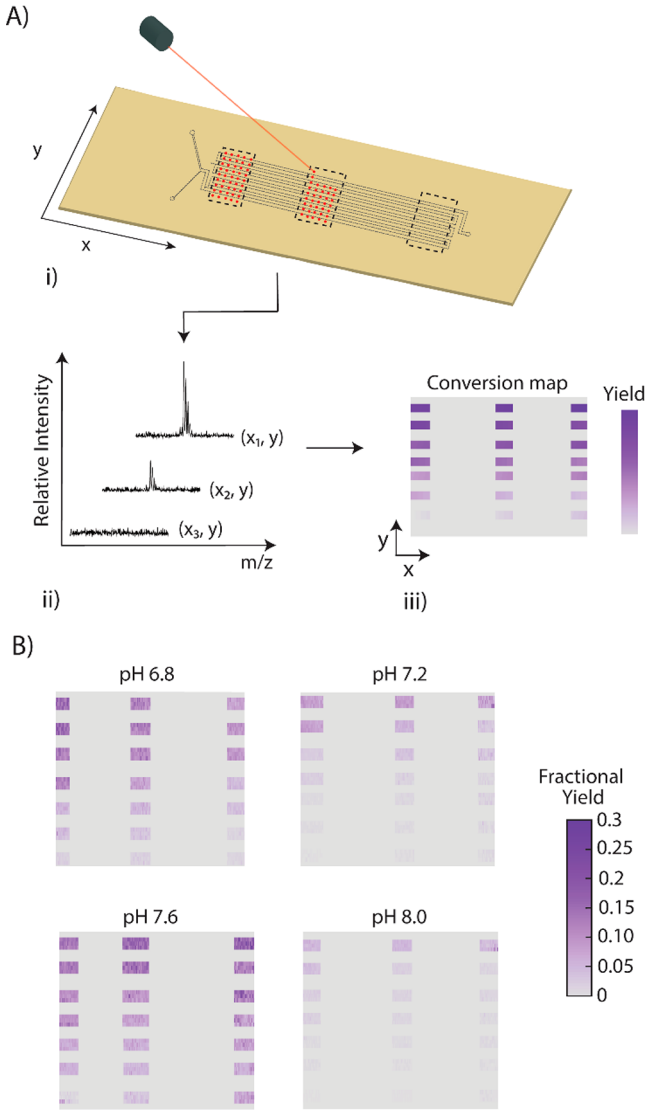

Figure 3. (A) iSAMDI-MS procedure. (i) Three regions on the chip are scanned with a MALDI-MS laser. (ii) Each spectrum represents a pixel in the region, and the product yield increases along the channel length. (iii) The fractional yield of product is extracted from each pixel and plotted into a heatmap. (B) Resulting heatmaps show the fractional product yield of the phenylglyoxal ligation reaction at pH 6.8, 7.2, 7.6, and 7.8.

Determining Fluid Velocity, Immobilization Rate, and Dispersion Characteristics. We determined the fluid velocity inside the channel to determine the exact relationship between position on the surface and reaction time in the channel. A solution of 1 mM fluorescein was injected into both inlets and flowed at a rate of 0.1 μL min^{-1}. We obtained images of the fluid front passing through a 12 mm × 12 mm region of the reactor at 30 s intervals with a confocal microscope (Figure 4A).

The average fluorescence intensities in 14 regions (each 200 μm × 600 μm) were plotted against time (Figure 4B, Figure S3). The resulting curves were fitted with a sigmoidal function, and the time at which the curves reached half the maximum intensity was plotted against the distance from the Y-junction (Figure 4C). We fitted the plot with linear regression to obtain the velocity of the fluid through the channel. The experimentally determined fluid velocity of 1.96 mm min^{-1} is

DOI: 10.1021/acscentsci.8b00867
ACS Cent. Sci. 2019, 5, 486−493

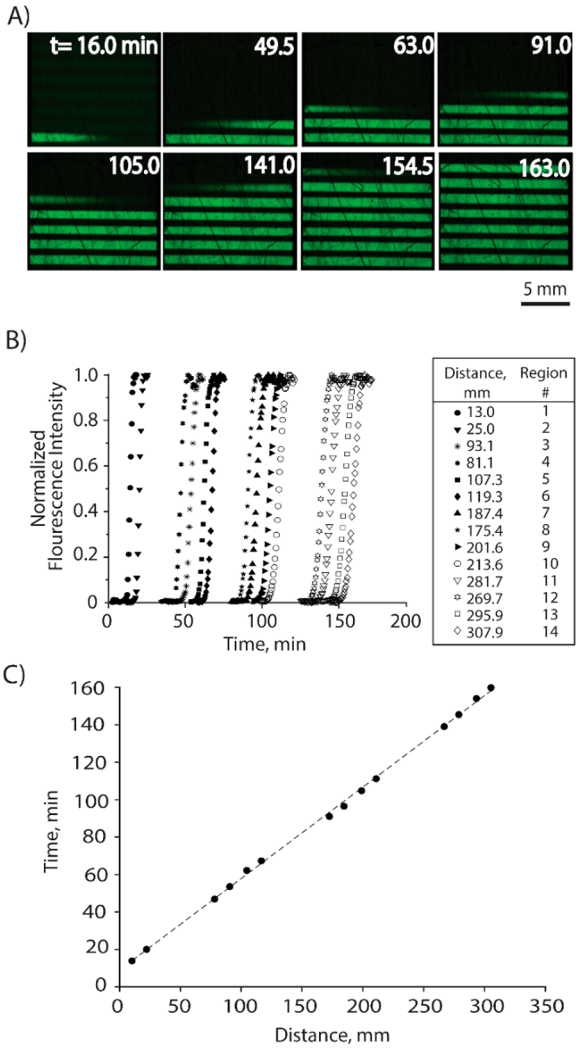

Figure 4. (A) Fluorescein was injected into the device channel at a concentration of 1 mM, and a confocal microscope was used to image the flow through the device. (B) Fluorescence intensity was monitored for 14 distinct regions in the channel. This plot shows the normalized fluorescence intensity, relative to time, for each position. The intensity plot at each region adopts a sigmoidal profile, characteristic of dispersion in the fluid front. (C) Plot of the time to half-maximum fluorescence intensity at the 14 regions versus their distance down the channel provides a linear relationship where the slope gives the fluid velocity. $R^2 = 0.99$, $y = 0.49x + 8.98$.

35% greater than the fluid velocity calculated from $Q = Av$, where Q is the volumetric flow rate, and A is the cross-sectional channel area. The 3D printed PDMS masters had rounded corners instead of sharp 90° edges, and light pressure was applied from an external clamp to keep the PDMS and chip together. We believe that both factors decreased the cross-sectional channel area and contributed to an increase in observed fluid velocity. To confirm that the determined fluid velocity matched that of the fit from the midpoint linear regression, and calculate the dispersion coefficient of the microfluidic device, we transformed the fluorescein flow profile from a sigmoidal function to a residence time distribution function (Figure S4). The average fluid velocity in the channel was calculated from the model to be 1.78 mm min^{-1}, which agrees well with the experimentally determined value. Recognizing that the residence time distribution function model properly details the unique characteristics of the dispersion front, and assuming that mass diffusion within the channel can be modeled as an instantaneous point-source, the dispersion coefficient was calculated to be 0.71 mm^2 s^{-1}, using Equation S2 in the Supporting Information. The calculated Peclet number was 836, suggesting that the convective flow of the fluid had a greater effect on the reaction rate than diffusive transport of the peptide species. Thus, the axial dispersion model (ADM) better describes this system.

To develop a complete understanding of the system, we experimentally determined the second-order rate constants for the reaction between the peptide and the maleimide on the surface. We used liquid handling robotics to dispense peptide solutions of varying concentrations and at 15 s intervals across 384-spot arrays presenting monolayers identical to those used in the microfluidic device. The reactions were rinsed from all spots after a fixed time, such that each spot recorded the immobilization yield for a unique reaction time. In this way, we generated kinetic profiles for the immobilization reaction over several peptide concentrations by performing SAMDI-MS and comparing the area under the curve of the unreacted maleimide to that of the peptide functionalized monolayer. Each concentration was fitted to a pseudo-first-order rate law, as the soluble peptide is present in great excess relative to the surface-bound maleimide. The pseudo-first-order rate constants were plotted against the concentration of peptide to determine the second-order rate constant for the immobilization reaction (Figure S5).

We determined the rate constants for immobilization to be 186, 263, 317, and 407 M^{-1} s^{-1} at pH values of 6.8, 7.2, 7.6, and 8.0, respectively. These data show that reaction of the thiols with maleimide is quite fast and that the rate increases with pH. These rapid immobilization rates also suggest that significant immobilization of reactants likely occurred in the region of the dispersion front, where the concentration of the reaction species was well below that of the concentrations in the steady state flow. We also calculated the Damköhler number for this reaction. The Damköhler number is a dimensionless parameter defined by the ratio of the rate of immobilization to the rate of convective mass transfer (eq 2):[15]

$$Da = \frac{kC_{a,0}^{n-1}}{\frac{u}{L}} \quad (2)$$

where k is the rate constant of immobilization, $C_{a,0}$ is the initial concentration of the reacting peptide species, n is the rate order of the immobilization reaction, L is the length of the channel, and u is the superficial velocity. We found the Damköhler number to be greater than 1 for all pH conditions described above, showing not only that the immobilization kinetics are fast, but also that immobilization to the surface is rapid relative to the flow rate in the channel. This further suggests that it is necessary for us to develop a model of immobilization to account for the effects of dispersion.

Incorporation of Dispersion with Immobilization Kinetics. We used MATLAB to produce a model that simulates the concentration profile of the phenylglyoxal ligation reaction species in the dispersion front. The model also uses the rate constant for immobilization to build a description of the immobilization kinetics which incorporates the concentration gradient found in the dispersive regime. We first used the rate law describing the immobilization of the reaction species to the floor of the channel (eq 3), where k is

DOI: 10.1021/acscentsci.8b00867
ACS Cent. Sci. 2019, 5, 486−493

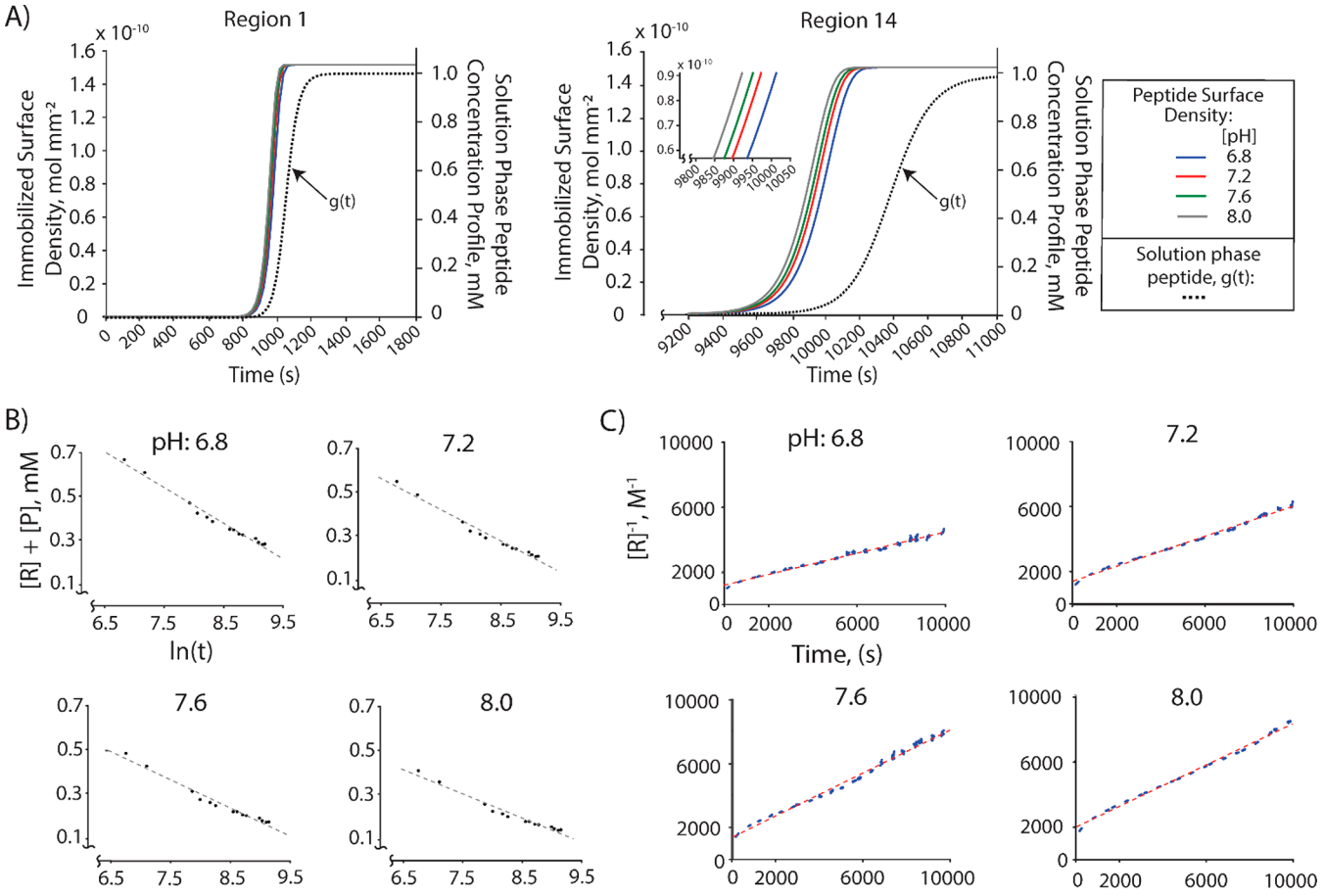

Figure 5. (A) Model of immobilization occurring in the channel that incorporates both dispersion and the experimentally determined rate constants for the reaction between the maleimide surface and solution-phase peptide. The plots show the pH-dependent immobilization (colored lines, left *y*-axis) alongside the solution-phase concentration and dispersion front (dashed line, right *y*-axis) for two fixed positions in the channel. Region 1 is a position early in the channel and region 14 is a position at the end of the channel (Figure S3). The inset highlights the effect of pH on the maleimide immobilization chemistry. Due to the rapid rate of immobilization, complete surface coverage is achieved before the dispersion front passes across the surface for all pH conditions. (B) Here, t = time in seconds. Across each pH condition, our model of immobilization kinetics was used to determine the solution-phase concentration of reaction species sampled by the surface. The plots presented here show the solution-phase concentration sampled by the surface as it relates to time (i.e., position in the channel). [R] + [P] represents the combined solution-phase concentration of reactant peptide and ligated peptide product. The concentration sampled by the surface adopts a logarithmic trend with respect to position in the channel, with the concentration sampled by the surface decreasing for positions further along the length of the channel. (C) The concentration sampled by the surface was multiplied by the fractional yield of the ligation reaction determined experimentally from imaging the channel floor with iSAMDI-MS. This gave the absolute yield of the ligation reaction for all positions imaged in the channel, which was plotted according to a standard second-order rate plot. The plots for each pH condition are seen here and adopt well behaved, linear relationships where the second-order rate constant is given by the slope.

the second-order rate constant for immobilization to the surface, Γ is the surface density of maleimide, and $g(t)$ represents the total concentration of the reaction species. We modeled $g(t)$ using the fluorescein imaging experiment presented in the previous section. The curves plotted in Figure 4B show normalized fluorescence intensity tracked at various positions along the channel as fluorescein was injected at a concentration matching that of the peptide in the ligation reactions. The sigmoidal shape of the curves is due to the dispersion front, and this front is elongated at positions further down the channel. Importantly, the fluorescence profiles demonstrate that the first region of interest used to quantitate the reaction progress occurs well past the chaotic mixing region of the channel inlet. To obtain $g(t)$, a standard 4-parameter sigmoidal function (eq 4) was fitted to these fluorescence profiles. The monolayers used in this work present maleimide-terminated alkanethiolates at an initial density of 1.53×10^{-10} mol cm^{-2} (Γ).[16]

$$\frac{d\Gamma}{dt} = -kg(t)\Gamma \tag{3}$$

$$g(t) = \frac{a + b}{1 + \left(\frac{t}{c}\right)^{d}} \tag{4}$$

Integration of eq 3 gives the kinetic model that describes the immobilization of the reaction species to the channel floor in the dispersive region of flow. In Figure 5A, we plot the time-dependent density of immobilized reaction species for each pH and at two fixed points in the channel (region 1 and region 14, representing positions near the beginning and end of the channel). The plots also show the solution-phase concentration profile, $g(t)$, for those same fixed positions in the channel.

DOI: 10.1021/acscentsci.8b00867
ACS Cent. Sci. 2019, 5, 486−493

This model shows that, in all cases, the immobilization reaction is completed before the bulk concentration is achieved in the flow (that is, before the dispersion front has passed over the surface). When looking at a position near the end of the channel, broadening of the dispersion front leads to an even greater deviation between the concentration sampled by the surface and the concentration in the bulk flow. Additionally, the time required for complete immobilization increases as the dispersion front elongates. As the pH of the reaction increases, the rate constant for immobilization also increases, leading to saturation of the surface at earlier points in the dispersion front (Figure S6).

Determination of Phenylglyoxal Ligation Kinetics. Finally, we used this model to analyze 14 positions in the channel for each pH condition, and to determine the time-weighted average concentration of reaction species during the immobilization at each position. To do so, we determined the time at which the reaction with the surface reached completion and then used this time as the upper limit for integration of the rate law (eq 3), giving the average concentration for the soluble reaction species at the surface (Figure 5B). In this analysis, time and position in the channel are equivalent representations of reaction progress.

Returning to the iSAMDI-MS heatmaps of the channel floors after the reaction, each pixel gives the fractional yield of the reaction at the corresponding position in the channel. To determine the second-order rate constant for the reaction of phenylglyoxal and the peptide in the channel, we first determined the concentration of the product in the channel (at each pixel) by multiplying the fractional yield observed by mass spectrometry by the concentration determined by our model. This concentration represents the yield of the ligation reaction at any given point in the channel. To determine the second-order reaction rate constant for the ligation reaction, we plotted the reciprocal of the concentration of the reactant peptide over time (Figure 5C). The slope of these plots gives the second-order rate constant of the reactions, which we determined to be 0.38 ± 0.06, 0.48 ± 0.04, 0.62 ± 0.05, and 0.62 ± 0.01 M^{-1} s^{-1}, at the respective pH values of 6.8, 7.2, 7.6, and 8.0. To assess the quality of our model, we performed similar reactions in bulk solution and analyzed the kinetics of those reactions using an identical SAMDI-MS strategy by pipetting a small amount of the reaction mixtures onto a monolayer array to generate reaction time points (Figure S7). We obtained rate constants from analysis of these bulk solution reactions which agree very well with those determined in the fluidic device.

These rates that we obtain are comparable to those for native chemical ligation reactions of thioesters and N-terminal cysteine residues.[17] Native chemical ligation also begins with nucleophilic attack by the thiol of a cysteine residue on a thioester, and competes with an irreversible thiol-to-amine acyl transfer. We observe that our reaction is pH-dependent, where an increase in pH from 6.8 to 7.6 yields an increase in rate, but an increase in pH from 7.6 to 8.0 leads to no significant change. The pK_a values of an N-terminal amine and cysteine are 8.0[18] and 8.5,[19] respectively, and explain our observed pH rate dependency.

DISCUSSION

In this work we demonstrate how iSAMDI-MS can be used to characterize the rate constant for a chemical reaction at a temporal resolution and with an amount of reactant that would be impractical to perform using current approaches. By performing reactions in flow and recording the reaction progress through covalent immobilization of the reactant and product to the floor of the channel, the temporal resolution is determined by the reaction flow rate and the spatial resolution of the MALDI mass spectrometer. Here, we image the surface at a pixel resolution of 200 μm, which corresponds to a temporal resolution of 6.1 s. Further, we acquired a total of 15 720 spectra and analyzed these data to obtain pH-dependent rate constants for the reaction between an N-terminal cysteine and phenylglyoxal.

One challenge with microfluidic devices is the dispersion zone that separates regions of fluid with different compositions. This is one reason why segmented flow methods have been developed to localize reagents into droplets or plugs.[20,21] Our approach was less compatible with the segmented formats because the monolayer must be in direct contact with the flowing reactants. However, the rapid immobilization kinetics for the reactants meant that we were not capturing product from the steady-state region of the flow but rather from the dispersion front. To relate the immobilization kinetics to the concentrations of these molecules in the flow, we developed a model that simulated the dispersion and used experimentally determined immobilization rate constants to simulate the amount of reactant and product that underwent immobilization. In this way, we could relate the density of product on the surface to the concentration of product in the steady state flow, and therefore we could extract the true second-order rate constant for the reaction. This work is significant because it describes the first microfluidic device operating under continuous flow that uses an in situ capture reaction to overcome dispersion.

A corresponding limitation of this approach is that it requires that the reactants and products contain a functional group to enable immobilization. The maleimide chemistry used in this work requires thiols for immobilization. However, we note that many other reactions, developed by our group and others, can be used for immobilization, including alkynes and azides, activated esters and amines, Diels–Alder reactants, and others.[9,22−27] We have also recently described a traceless immobilization method that uses a photogenerated carbene to rapidly and covalently immobilize a broad range of molecules, and this may serve as a more generalizable immobilization strategy in future applications.[28] We note that it will be important to verify that both the reactant and product undergo immobilization to the monolayer with the same rate constant—or to determine rate constants for each molecule—so that the immobilized fraction can be related to relative concentrations in solution. Hence, we anticipate many ways in which the methodology described here can be applied to other reactions.

By integrating the reaction steps with product isolation in a single device, we simplify the analysis of rate constants and minimize manual reagent handling. Previous combinations of microfluidic systems and mass spectrometry have required the collection of the reaction products by arraying on a second substrate (for MALDI-MS) or directly interfacing the device with a mass spectrometer. Both are time-consuming and can generate uncertainty in the kinetic profile if the reactions are not adequately quenched or are not sampled properly. In addition, it is difficult to integrate bulky equipment with microfluidic devices. Here, we simply rinse out the remaining reagent from the fluidic device, remove the chip entirely from

DOI: 10.1021/acscentsci.8b00867
ACS Cent. Sci. 2019, 5, 486−493

the fluidic element, and acquire iSAMDI-MS directly from the chip.

The combination of flow rate and channel length will determine the reaction times that can be analyzed in the microfluidic device. The mass spectrometer we used in this work can analyze substrates with a size corresponding to a standard multiwell plate (~100 cm^2) and can therefore accommodate devices having very long channel lengths. We estimate that the approach can be used to measure reactions with half-lives ranging from several minutes to several hours.

Finally, we note the efficiency that this approach offers in performing high-throughput experiments. We acquired approximately 1200 data points from each device using 12 μL of reagent, which corresponds to 10 nL of reagent for each data point. Current commercial mass spectrometers can perform iSAMDI-MS at a resolution of over 15 million data points with 10 μm pixel resolution. Reactions that consume picoliter volumes of reagent will be possible with devices that contain nanometer-scale channels and reaction wells.[29,30] In addition, devices can be designed to contain multiple reaction channels for parallel reaction screening.

In summary, we developed an approach based on SAMDI mass spectrometry that performs high-throughput experiments in microfluidic cells to determine the rate constant for a chemical reaction. This approach is enabled by the use of self-assembled monolayers on the floor of the channels, which allows for both selective immobilization of reactants and direct analysis by SAMDI mass spectrometry. This approach allows for massively parallel experimentation using minimal reagent and does not require tedious approaches for isolating reaction products or for labels used to quantitate products. We expect that this and related work will find use in combinatorial chemistry and drug screening applications.

MATERIALS AND METHODS

Amino acids and peptide synthesis reagents were purchased from Anaspec. The peptide was prepared using standard Fmoc solid-phase synthesis methods on Rink Amide MBHA resin and purified with high-performance liquid chromatography (HPLC).[31] Phenylglyoxal hydrate and fluorescein sodium salt was obtained from Sigma-Aldrich. PDMS prepolymer mixture was purchased from Ellsworth Adhesives. No unexpected or unusually high safety hazards were encountered.

iSAMDI-MS was obtained on an AutoFlex-III MALDI-ToF instrument with SmartBeam-II laser (Bruker Daltonics). Fluorescence video imaging was acquired with a confocal Nikon Ti Eclipse (Nikon) microscope.

ASSOCIATED CONTENT

Supporting Information

The Supporting Information is available free of charge on the ACS Publications website at DOI: 10.1021/acscentsci.8b00867.

Detailed procedures for microfluidic device fabrication and operation, iSAMDI-MS acquisition, flow velocity determination, immobilization kinetics determination, dispersion coefficient calculation, convective flow analyses, and the MATLAB code used (PDF)

AUTHOR INFORMATION

Corresponding Author

*E-mail: milan.mrksich@northwestern.edu.

ORCID

Patrick T. O'Kane: 0000-0002-2187-6760

Milan Mrksich: 0000-0002-4964-796X

Author Contributions

‖J.G. and P.T.O. contributed equally.

Notes

The authors declare no competing financial interest.

ACKNOWLEDGMENTS

J.G. and B.R.K. were supported by the National Science Foundation Graduate Research Fellowship under Grants DGE-1324585 and DGE-1842165, respectively. We acknowledge support from the Department of the Defense, Defense Threat Reduction Agency HDTRA1-15-1-0052. This work used facilities of the Integrated Molecular Structure Education and Research Center, the 3D Printing & Rapid Prototyping Lab, the Structural Biology Core, and the Research Shop—Instrumentation Design, Engineering & Production.

REFERENCES

(1) Huebner, A. M.; Abell, C.; Huck, W. T. S.; Baroud, C. N.; Hollfelder, F. Monitoring a Reaction at Submillisecond Resolution in Picoliter Volumes. *Anal. Chem.* **2011**, *83* (4), 1462−1468.

(2) Mao, H.; Yang, T.; Cremer, P. S. A Microfluidic Device with a Linear Temperature Gradient for Parallel and Combinatorial Measurements. *J. Am. Chem. Soc.* **2002**, *124* (16), 4432−4435.

(3) Fidalgo, L. M.; Whyte, G.; Ruotolo, B. T.; Benesch, J. L. P.; Stengel, F.; Abell, C.; Robinson, C. V.; Huck, W. T. S. Coupling Microdroplet Microreactors with Mass Spectrometry: Reading the Contents of Single Droplets Online. *Angew. Chem., Int. Ed.* **2009**, *48* (20), 3665−3668.

(4) Wang, J.; Sui, G.; Mocharla, V. P.; Lin, R. J.; Phelps, M. E.; Kolb, H. C.; Tseng, H.-R. Integrated Microfluidics for Parallel Screening of an In Situ Click Chemistry Library. *Angew. Chem., Int. Ed.* **2006**, *45* (32), 5276−5281.

(5) Browne, D. L.; Wright, S.; Deadman, B. J.; Dunnage, S.; Baxendale, I. R.; Turner, R. M.; Ley, S. V. Continuous Flow Reaction Monitoring Using an On-Line Miniature Mass Spectrometer. *Rapid Commun. Mass Spectrom.* **2012**, *26* (17), 1999−2010.

(6) Liu, Y.; Ismagilov, R. F. Dynamics of Coalescence of Plugs with a Hydrophilic Wetting Layer Induced by Flow in a Microfluidic Chemistrode. *Langmuir* **2009**, *25* (5), 2854−2859.

(7) Hatakeyama, T.; Chen, D. L.; Ismagilov, R. F. Microgram-Scale Testing of Reaction Conditions in Solution Using Nanoliter Plugs in Microfluidics with Detection by MALDI-MS. *J. Am. Chem. Soc.* **2006**, *128* (8), 2518−2519.

(8) Bula, W. P.; Verboom, W.; Reinhoudt, D. N.; Gardeniers, H. J. G. E. Multichannel Quench-Flow Microreactor Chip for Parallel Reaction Monitoring. *Lab Chip* **2007**, *7* (12), 1717−1722.

(9) Houseman, B. T.; Gawalt, E. S.; Mrksich, M. Maleimide-Functionalized Self-Assembled Monolayers for the Preparation of Peptide and Carbohydrate Biochips. *Langmuir* **2003**, *19* (5), 1522−1531.

(10) Weber, A. L. Formation of the Thioester, N-Acetyl, S-Lactoylcysteine, by Reaction of N-Acetylcysteine with Pyruvaldehyde in Aqueous Solution. *J. Mol. Evol.* **1982**, *18* (5), 354−359.

(11) Okuyama, T.; Komoguchi, S.; Fueno, T. Reaction of Thiols with Phenylglyoxal to Give Thiol Esters of Mandelic Acid. II. Intramolecular General-Base Catalysis and Change in Rate-Determining Step. *J. Am. Chem. Soc.* **1982**, *104* (9), 2582−2587.

(12) Dawson, P. E.; Muir, T. W.; Clark-Lewis, I.; Kent, S. B. Synthesis of Proteins by Native Chemical Ligation. *Science* **1994**, *266* (5186), 776−779.

(13) Grant, J.; Modica, J. A.; Roll, J.; Perkovich, P.; Mrksich, M. An Immobilized Enzyme Reactor for Spatiotemporal Control over Reaction Products. *Small* **2018**, *14* (31), 1800923.

(14) Grant, J.; Goudarzi, S. H.; Mrksich, M. High-Throughput Enzyme Kinetics with 3D Microfluidics and Imaging SAMDI Mass Spectrometry. *Anal. Chem.* **2018**, *90* (21), 13096−13103.
(15) Fernandes del Pozo, D. Effect of Mass Transfer Limitations on Enzymatic Reactions in Microreactors: a Model-Based Analysis. Masters Dissertation, Ghent University, Belgium, 2015.
(16) Liao, X.; Su, J.; Mrksich, M. An Adaptor Domain-Mediated Autocatalytic Interfacial Kinase Reaction. *Chem. - Eur. J.* **2009**, *15* (45), 12303−12309.
(17) Pollock, S. B.; Kent, S. B. H. An Investigation into the Origin of the Dramatically Reduced Reactivity of Peptide-Prolyl-Thioesters in Native Chemical Ligation. *Chem. Commun.* **2011**, *47* (8), 2342−2344.
(18) Chen, D.; Disotuar, M. M.; Xiong, X.; Wang, Y.; Chou, D. H.-C. Selective N-Terminal Functionalization of Native Peptides and Proteins. *Chem. Sci.* **2017**, *8* (4), 2717−2722.
(19) Britto, P. J.; Knipling, L.; Wolff, J. The Local Electrostatic Environment Determines Cysteine Reactivity of Tubulin. *J. Biol. Chem.* **2002**, *277* (32), 29018−29027.
(20) Song, H.; Chen, D. L.; Ismagilov, R. F. Reactions in Droplets in Microfluidic Channels. *Angew. Chem., Int. Ed.* **2006**, *45* (44), 7336−7356.
(21) Mark, D.; Haeberle, S.; Roth, G.; von Stetten, F.; Zengerle, R. Microfluidic Lab-on-a-Chip Platforms: Requirements, Characteristics and Applications. *Chem. Soc. Rev.* **2010**, *39* (3), 1153−1182.
(22) Yousaf, M. N.; Mrksich, M. Diels−Alder Reaction for the Selective Immobilization of Protein to Electroactive Self-Assembled Monolayers. *J. Am. Chem. Soc.* **1999**, *121* (17), 4286−4287.
(23) Ban, L.; Pettit, N.; Li, L.; Stuparu, A. D.; Cai, L.; Chen, W.; Guan, W.; Han, W.; Wang, P. G.; Mrksich, M. Discovery of Glycosyltransferases Using Carbohydrate Arrays and Mass Spectrometry. *Nat. Chem. Biol.* **2012**, *8* (9), 769−773.
(24) Ban, L.; Mrksich, M. On-Chip Synthesis and Label-Free Assays of Oligosaccharide Arrays. *Angew. Chem.* **2008**, *120* (18), 3444−3447.
(25) Wollman, E. W.; Kang, D.; Frisbie, C. D.; Lorkovic, I. M.; Wrighton, M. S. Photosensitive Self-Assembled Monolayers on Gold: Photochemistry of Surface-Confined Aryl Azide and Cyclopentadienylmanganese Tricarbonyl. *J. Am. Chem. Soc.* **1994**, *116* (10), 4395−4404.
(26) Chechik, V.; Crooks, R. M.; Stirling, C. J. M. Reactions and Reactivity in Self-Assembled Monolayers. *Adv. Mater.* **2000**, *12* (16), 1161−1171.
(27) Diagne, A. B.; Li, S.; Perkowski, G. A.; Mrksich, M.; Thomson, R. J. SAMDI Mass Spectrometry-Enabled High-Throughput Optimization of a Traceless Petasis Reaction. *ACS Comb. Sci.* **2015**, *17* (11), 658−662.
(28) Helal, K. Y.; Alamgir, A.; Berns, E. J.; Mrksich, M. Traceless Immobilization of Analytes for High-Throughput Experiments with SAMDI Mass Spectrometry. *J. Am. Chem. Soc.* **2018**, *140* (26), 8060−8063.
(29) Tyagi, S.; VanDelinder, V.; Banterle, N.; Fuertes, G.; Milles, S.; Agez, M.; Lemke, E. A. Continuous Throughput and Long-Term Observation of Single-Molecule FRET without Immobilization. *Nat. Methods* **2014**, *11* (3), 297−300.
(30) Bouilly, D.; Hon, J.; Daly, N. S.; Trocchia, S.; Vernick, S.; Yu, J.; Warren, S.; Wu, Y.; Gonzalez, R. L.; Shepard, K. L.; et al. Single-Molecule Reaction Chemistry in Patterned Nanowells. *Nano Lett.* **2016**, *16* (7), 4679−4685.
(31) Kilian, K. A.; Mrksich, M. Directing Stem Cell Fate by Controlling the Affinity and Density of Ligand-Receptor Interactions at the Biomaterials Interface. *Angew. Chem., Int. Ed.* **2012**, *51* (20), 4891−4895.

DOI: 10.1021/acscentsci.8b00867
ACS Cent. Sci. 2019, 5, 486−493